XLVI CILAMCE
VITÓRIA - ES - BRAZIL - 2025
XLVI IBERO-LATIN AMERICAN CONGRESS ON COMPUTATIONAL METHODS IN ENGENEERING

234 - Comparative analysis of boundary treatments and regularization orders in GPU-based lattice Boltzmann simulations

Bruno Y. dos Anjos[1], Gustavo T. Choaire[1], Luiz A. Hegele Jr.[1]

[1]*Dept. of Petroleum Engineering, Santa Catarina State University*
Avenida Lourival Cesario Pereira, 88336-275, Santa Catarina, Brazil
bruno.anjos@edu.udesc.br, gustavo.choaire@udesc.br, luiz.hegele@udesc.br

Abstract. We present a two-dimensional GPU-accelerated implementation of the lattice Boltzmann method (LBM) using CUDA, tailored for computational fluid dynamics applications. The numerical framework employs the D2Q9 velocity stencil combined with a regularized Bhatnagar-Gross-Krook collision operator. Our primary objective is the systematic evaluation and optimization of distinct LBM formulations through detailed comparisons between second-order and high-order regularization, extending the analysis to include implementations up to fourth-order moments. Such high-order regularization are instrumental in enhancing numerical stability and accuracy. Additionally, the impact of different boundary condition approaches is rigorously assessed through comparative studies between regularized boundary conditions and incompressible regularized boundary conditions. The computational performance and numerical accuracy of each approach are investigated using the classical lid-driven cavity flow configuration as a standard benchmark problem. Exploiting the computational advantages inherent in two-dimensional simulations, we utilize high-resolution grids consisting of 1024 and 2048 lattice points. These simulations are conducted across a comprehensive range of Reynolds numbers (3,200, 10,000, 50,000, and 100,000), thus demonstrating the robustness of the solver and capability in accurately resolving complex flow features typical of highly inertial regimes.

Keywords: Lattice Boltzmann Method, GPU Computing, High-order Regularization, Lid-driven Cavity.

1 Introduction

The study of fluid mechanics plays a fundamental role in understanding natural phenomena, as it is widely applicable across various branches of science and technology [1, 2]. To improve the understanding and prediction of fluid behavior, the field of computational fluid dynamics (CFD) has been developed. In the present research, the lattice Boltzmann method (LBM) is employed due to its proven effectiveness in simulating turbulent flows, which are often challenging to model with conventional methods [3].

In order to improve computational efficiency, a GPU-based implementation using CUDA was developed, allowing the exploitation of massive parallelism to accelerate simulations without compromising accuracy or stability [4]. The lattice Boltzmann method (LBM) is inherently parallel due to its localized operations: computations at each lattice site are performed independently, and inter-site communication only occurs during the streaming step. This step can be efficiently handled using domain decomposition strategies, in which subdomains—referred to as blocks in GPU implementations—are distributed across the device, as proposed by Ferrari et al. [4]. Therefore, it becomes evident that the LBM is particularly well-suited for high-Reynolds-number simulations on GPUs, fulfilling both performance and scalability requirements.

The collision step governs the evolution of the distribution function at each lattice site. Among all collision methods, the Bhatnagar-Gross-Krook (BGK) collision operator is employed in the present study. The BGK model assumes that the distribution function relaxes toward its equilibrium state at a rate determined by a relaxation time constant [5, 6].

Several techniques are employed to enhance computational efficiency in comparison to the classical LBM scheme. The main objective of this work is to evaluate the impact of such approaches in terms of computational effort, accuracy, and stability within a two-dimensional implementation. We begin by outlining the strategies already implemented.

Two key approaches are considered. The first is the regularized LBM, in which the distribution functions are expressed as functions of moments and microscopic velocities, leading to improved numerical stability [3, 7]. The

second is the moment-based LBM, where only the moments are stored and used in the collision process instead of the distribution functions, which significantly increases computational efficiency in the simulations [8].

On the other hand, this work also investigates the effects of high-order regularization and varied boundary treatments, specifically regularized boundary conditions (RBC) and incompressible regularized boundary conditions (IRBC), on the simulation results. All boundary conditions are prescribed in terms of velocity, a type commonly referred to as Dirichlet conditions. For this purpose, the lid-driven cavity (LDC) flow is chosen as the benchmark geometry [3, 9–12].

A compelling reason for choosing the lid-driven cavity (LDC) flow as the reference geometry lies in its ability to capture complex and turbulent bounded flow behavior, while maintaining a relatively simple boundary configuration. In this setup, all walls are treated as no-slip boundaries, with the exception of the top wall, which moves at a constant velocity; the remaining walls are stationary.

Moreover, the LDC flow has been extensively investigated using a wide range of numerical methods, including lattice Boltzmann formulations, making it a well-established benchmark for validating and comparing simulation results [3, 4, 9].

2 Methods

To address the proposed problem, the lattice Boltzmann method (LBM) is employed to generate the results presented in this work. This method models fluid behavior by discretizing the domain into a set of points, referred to as lattice nodes. Each node holds a set of distribution functions, denoted by f_i, which represent the particle density in predefined discrete velocity directions. These directions vary according to the chosen velocity set, commonly referred to as velocity stencils [13–15]. The entire process, consisting of streaming and collision, is expressed as:

$$f_i\left(\boldsymbol{x}+\boldsymbol{c}_i\Delta t, t+\Delta t\right) = f_i\left(\boldsymbol{x}, t\right) + \Omega_i\left(\boldsymbol{x}, t\right), \tag{1}$$

where $\boldsymbol{c}_i$ denotes the microscopic velocity vector, and $\boldsymbol{x}$ represents the spatial position within the lattice. In this work, the Bhatnagar-Gross-Krook (BGK) collision operator is employed. This model assumes that each distribution function relaxes toward its equilibrium value, with the relaxation governed by a time constant τ, known as the relaxation time [6]. The BGK collision operator is defined as:

$$\Omega_i\left(\boldsymbol{x}, t\right) = -\frac{\Delta t}{\tau}\left(f_i\left(\boldsymbol{x}, t\right) - f_i^{eq}\left(\boldsymbol{x}, t\right)\right). \tag{2}$$

The relaxation time τ can be determined through its correlation with the kinematic viscosity ν. This relationship is derived from the Chapman–Enskog expansion, which establishes a formal connection between the Lattice Boltzmann Equation (LBE) and the Navier–Stokes Equations (NSE) [16]. Accordingly, the kinematic viscosity is given by:

$$\nu = a_s^{-2}\left(\tau - \frac{\Delta t}{2}\right), \tag{3}$$

In the previous equation, a_s denotes the scaling factor, which is defined to ensure that the microscopic velocity vectors $\boldsymbol{c}_i$ are normalized. In the LBM framework, macroscopic moments can be directly associated with the distribution functions by combining them with the microscopic velocities [3, 9]. In the classical formulation, three fundamental moments are commonly defined: the zeroth-order moment, first-order moment, and second-order moment. These correspond physically to the fluid density, momentum, and the strain rate tensor, respectively. The first-order moment is represented by ρ, followed by ρu_α and $\rho m^{(2)}_{\alpha\beta}$. These moments are expressed as:

$$\left\{\rho, \rho u_\alpha, \rho m^{(2)}_{\alpha\beta}\right\} = \sum_i f_i\left\{1, c_{i\alpha}, H^{(2)}_{\alpha\beta,i}\right\}, \tag{4}$$

where $H_{\alpha\beta} = c_{i\alpha}c_{i\beta} - \delta_{\alpha\beta}/a_s^2$ is the Hermite polynomial function, employed in the LBM due to its orthogonality property. and the term $\delta_{\alpha\beta}$ denotes the Kronecker delta. Since the present work adopts a regularized LBM formulation, this representation becomes particularly important. Both the regularized distribution functions, denoted by $\hat{f}_i$, and the equilibrium distribution functions are expressed in terms of their respective moments [7], as follows:

$$\hat{f}_i = \rho w_i\left(1 + a_s^2 u_\alpha c_{i\alpha} + \frac{a_s^4}{2} m^{(2)}_{\alpha\beta} H^{(2)}_{\alpha\beta,i}\right), \tag{5}$$

$$f_i^{eq} = \rho w_i\left(1 + a_s^2 u_\alpha c_{i\alpha} + \frac{a_s^4}{2} u_\alpha u_\beta H^{(2)}_{\alpha\beta,i}\right). \tag{6}$$

The variable w_i represents the weighting factor associated with a given lattice direction. This weight corresponds to the probability of particle propagation in that direction and plays a crucial role in predicting flow behavior at each lattice node. The values of w_i are determined using Gauss quadrature and depend on the chosen velocity stencil [17].

The primary objectives of this work are to investigate the computational behavior of two-dimensional flows under high-order regularization and to analyze the impact of different boundary condition treatments. To achieve these goals, the lid-driven cavity (LDC) flow is employed as the reference geometry, due to its well-established use in benchmarking complex fluid flow behavior with relatively simple boundary conditions [3].

Since this study is focused on a two-dimensional case, the D2Q9 stencil is adopted for all simulations. The following sections present the approaches used to address the proposed problem.

2.1 Moment representation

The moment representation is a technique used to reduce the computational cost of simulations. This approach is based on storing only the relevant moments at each lattice site, rather than the full set of population functions. In a two-dimensional simulation, such as the one presented in this work, the memory savings are directly proportional to the number of variables stored per lattice node [8, 18].

To compute the collided moments, we use eq. (1) in combination with eq. (2), where the post-collision values are denoted by an asterisk (*). Under this formulation, the collision step in moment space can be expressed as:

$$m^{*}_{\alpha\beta} = (1-\omega)m^{(2)}_{\alpha\beta} + \omega u_\alpha u_\beta, \tag{7}$$

where $\omega = \Delta t/\tau$. Once the collided moments are computed, the distribution functions can be reconstructed using Eq. (5), after which they are streamed to neighboring nodes, repeating the process.

2.2 High Order Regularization

A high-order expansion is obtained when the distribution function is not truncated at the second-order term. In this context, the full definition of the regularized distribution function can be exploited to improve accuracy [11, 12, 17].

We uses the approach proposed by Malaspinas [11], higher-order moments—such as third or fourth order—can be expressed as functions of second-order moments through the use of non-equilibrium distribution functions. The thrid and fourth order moments can be expressed as:

$$m^{(neq)}_{\alpha_1\alpha_2\alpha_3} = u_{\alpha_3} m^{(neq)}_{\alpha_1\alpha_2} + u_{\alpha_2} m^{(neq)}_{\alpha_1\alpha_3} + u_{\alpha_1} m^{(neq)}_{\alpha_2\alpha_3}, \tag{8}$$

$$m^{(neq)}_{\alpha_1\alpha_2\alpha_3\alpha_4} = u_{\alpha_4} m^{(neq)}_{\alpha_1\alpha_2\alpha_3} + u_{\alpha_1} u_{\alpha_2} m^{(neq)}_{\alpha_3\alpha_4} + u_{\alpha_1} u_{\alpha_3} m^{(neq)}_{\alpha_2\alpha_4} + u_{\alpha_2} u_{\alpha_3} m^{(neq)}_{\alpha_1\alpha_4}. \tag{9}$$

2.3 Boundary Conditions

Regularized Boundary Condition (RBC) method offers a robust framework for addressing the physical constraints of the flow. This approach was first introduced by Hegele Jr et al. [3], who applied the regularization process to reconstruct the missing distribution functions at the boundaries. The expressions proposed for this system of equations are given by:

$$\rho_I = \sum_{i\in I_s} f_i = (1-\omega) \sum_{i\in O_s} \hat{f}_i + \omega \sum f^{eq}_i, \tag{10}$$

$$\rho_I m^{(2)}_{\alpha\beta,I} = \sum_{i\in I_s} f_i H^{(2)}_{\alpha\beta,i} = \sum_{i\in I_s} \hat{f}_i H^{(2)}_{\alpha\beta,i}, \tag{11}$$

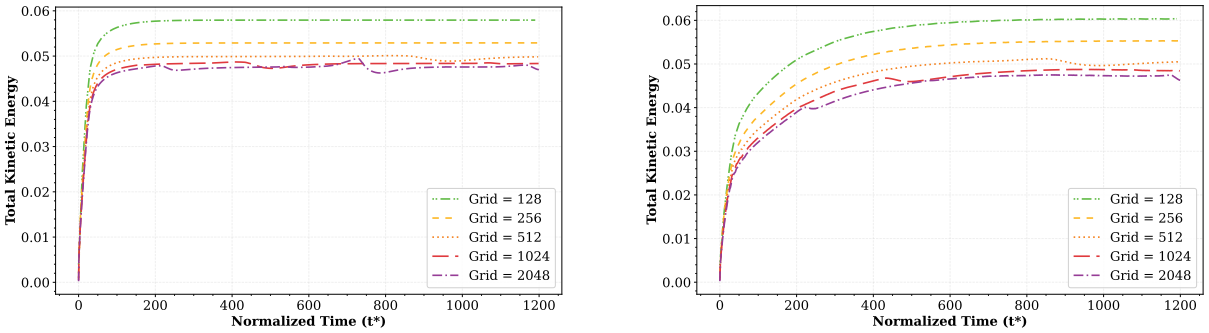
where I represents the incoming moments at a given lattice site, and I_s and O_s denote the sets of incoming and outgoing distribution functions, respectively, at each boundary node. Further details on the definition of incoming and outgoing directions can be found in [3].

An incompressible flow assumption is also adopted in this work. Under this assumption, the system can be further simplified, as the second-order moments can be directly expressed as functions of the velocity components. For example, $m^{(2)}_{xx} = u^2_x$ and $m^{(2)}_{yy} = u^2_y$ [9].

3 Validation

To validate the results, comparisons are made with the benchmark data provided by Ghia et al. [19]. As the objective of the present study is to evaluate the model under more demanding conditions, only high Reynolds numbers are considered. Specifically, simulations are performed for $Re = 3200$ and $Re = 10000$.

To determine when the flow reaches a steady state, the evolution of the total kinetic energy is analyzed. This quantity is computed per unit mass using the expression $\sum u^2/(2U_{\text{lid}}^2 N_x N_y)$, where it serves as a valuable indicator of both flow behavior and computational accuracy.We uses non-dimensional time measured by $t^* = tU_{\text{lid}}/N_x$.



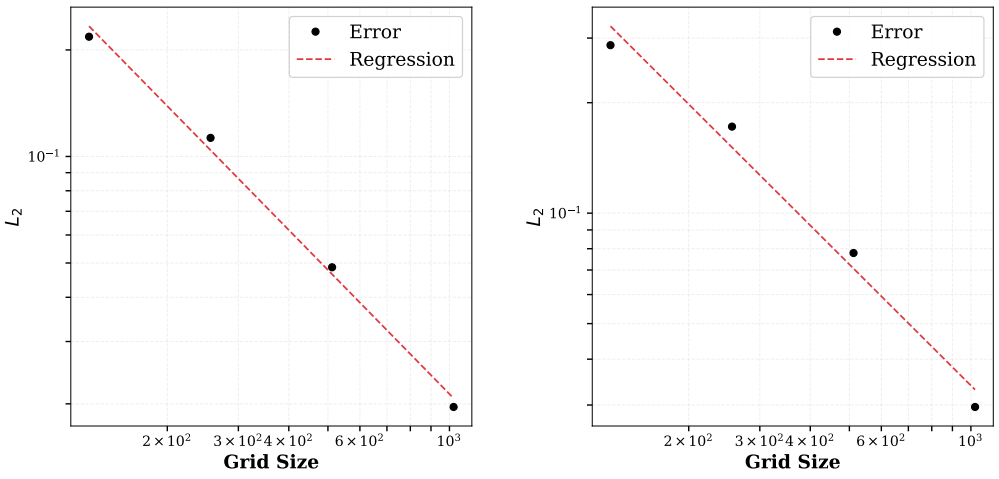
(a) $Re = 3{,}200$ (b) $Re = 10{,}000$

Figure 1. Total kinetic energy per unity of mass normalized

Figure 1 presents the total kinetic energy (TKE) evolution for both validation cases, corresponding to Reynolds numbers of 3,200 and 10,000. As no significant variations in kinetic energy are observed over time, it can be assumed that the flow has reached a steady state. Consequently, the velocity field can be extracted for comparison with benchmark results from the literature.

It is important to note that, since the present study involves a two-dimensional simulation, the turbulent features typically associated with these Reynolds numbers are not expected to develop. This explains why the kinetic energy stabilizes, a behavior that would not generally occur in three-dimensional simulations.

In addition to verifying the steady state, grid convergence is analyzed with respect to mesh refinement. This can be qualitatively observed when the kinetic energy curves for different grids overlap or intertwine, indicating that the flow behavior is being similarly represented across varying resolutions.



(a) $Re = 3{,}200$ (b) $Re = 10{,}000$

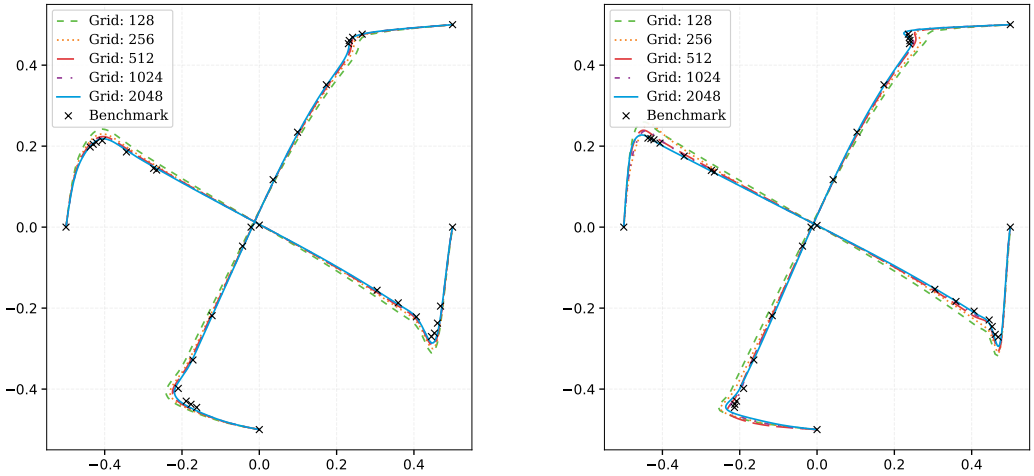
Figure 2. L_2 error for both Reynolds number

Because visual inspection is qualitative, a quantitative assessment is introduced through the L_2 norm of the error, computed between the kinetic energy profiles of coarser grids and the reference case, represented by the finest grid. This error corresponds to the square root of the sum of squared differences between each profile

and the reference. As shown in Fig. 2, the error decreases noticeably with increasing grid resolution, reflecting improved solution accuracy—a trend both expected and desirable. The slopes of the error curves are approximately -1.12 for $Re = 3{,}200$ and -1.04 for $Re = 10{,}000$, evaluated over the interval from $t^* = 600$ onwards in order to minimize numerical artifacts such as the oscillations observed in Fig. 1. When the error is instead evaluated only at the final value of the TKE, the slopes become -1.21 for $Re = 3{,}200$ and -1.07 for $Re = 10{,}000$.

An additional test was performed by excluding the coarsest grid (128×128) from the slope calculation. In this case, the average approach yields slopes of -1.18 for $Re = 3{,}200$ and -1.21 for $Re = 10{,}000$. The single-point comparison at the end of the TKE further increases the slopes to -1.30 and -1.21 for $Re = 3{,}200$ and $Re = 10{,}000$, respectively.

Although these slopes remain below the ideal value of -2, they are acceptable for the present study. A plausible explanation for the reduced convergence rate is that the grid resolution is already sufficiently fine for moderate Reynolds numbers, limiting the gain in accuracy with further refinement. To complement this validation analysis, velocity profiles were extracted after $12{,}000$ non-dimensional time steps, ensuring that steady-state conditions had been fully established.



(a) $Re = 3{,}200$ (b) $Re = 10{,}000$

Figure 3. Velocity profile on the centerline, on the horizontal centerline velocity on y direction, on vertical centerline the value of the velocity on direction x

Figure 3 demonstrates excellent agreement between the velocity profiles obtained in this study and those reported by Ghia et al. [19]. This is particularly relevant in validating the consistency of the LBM, as the benchmark data in the literature are based on direct solutions of the Navier–Stokes equations (NSE). The ability of the proposed LBM formulation to reproduce these reference results highlights its accuracy and effectiveness.

To ensure a proper comparison, both the velocity and spatial coordinates were normalized and scaled. Velocities were halved and coordinates were shifted by half the total domain size, allowing all curves to fit within the normalized range of -0.5 to 0.5.

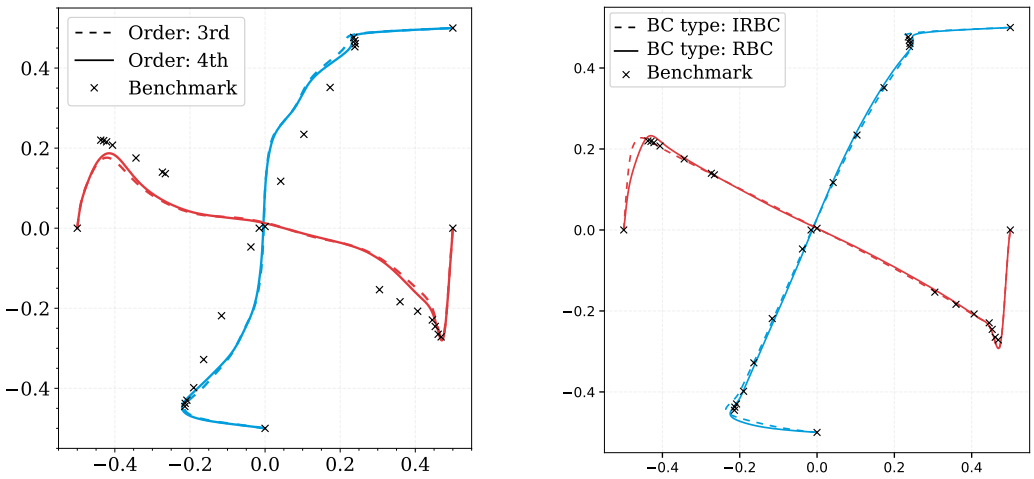
These investigations also confirm that the quality of the results improves with grid refinement, in agreement with all previous observations. This supports the motivation behind the present work: to explore high-resolution simulations at elevated Reynolds numbers and analyze the computational behavior of the method under such conditions.

4 Results

To evaluate the effects of high-order regularization and different boundary condition treatments, simulations were performed at a Reynolds number of $10{,}000$. This choice provides a challenging yet meaningful benchmark for comparison, allowing for the extraction of reliable and insightful observations.

On the other hand, the high Reynolds number simulations are also intended to explore how such flows can be effectively approached and evaluated. The techniques adopted in this study can be extended to three-dimensional schemes in a straightforward manner.

In the following section, we present the velocity fields corresponding to the high-order regularization and boundary treatment results.



(a) High order effect

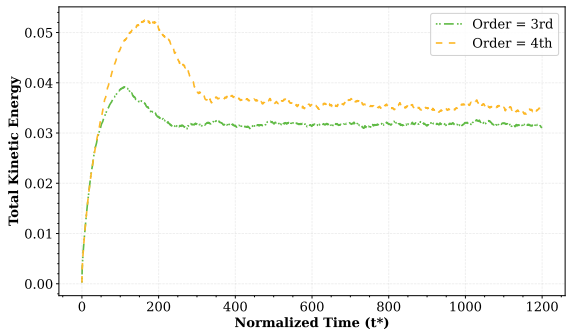
(b) Boundary effect

Figure 4. The blue plot represents the value of u_x along vertical centerline, while the red plot represents the value of u_y towards the horizontal centerline

Figure 5a allows for the evaluation of the high-order regularization performance. From a computational perspective, the high-order formulation does not introduce any significant performance degradation, with simulation times remaining nearly equivalent to those of the second-order case.

However, the velocity fields reveal noticeable deviations, particularly in the central region of the cavity. In contrast, the results near the boundaries show excellent agreement with the second-order solution, indicating that high-order regularization maintains good accuracy at the walls.

One striking feature of the high-order simulations is the behavior of the total kinetic energy. Unlike the second-order results, the high-order formulation exhibits substantial fluctuations in kinetic energy over time, as illustrated in Fig. 5.



(a) High order effect

Figure 5. Total kinetic energy per unity of mass normalized

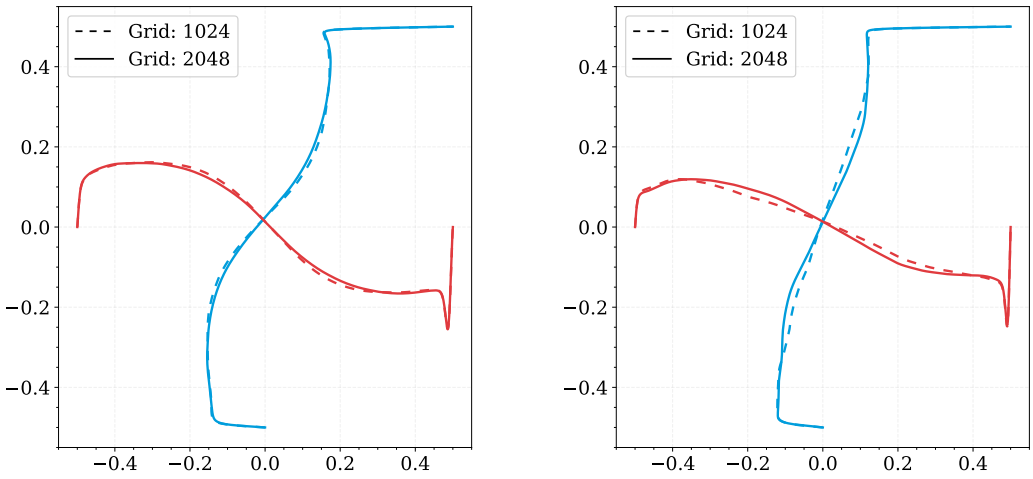
The observed results may be attributed to numerical instabilities, or alternatively, they may reflect distinct flow behavior introduced by the high-order formulation. This uncertainty necessitated the use of a time-averaged velocity field, rather than relying on a single snapshot after the flow reaches steady state. This time-averaging procedure helps to explain the discrepancies observed when comparing high-order results to those obtained using second-order formulations.

When analyzing the results shown in Fig. 4b, it is evident that the velocity fields obtained using RBC and IRBC boundary conditions are very similar. In fact, IRBC yields slightly better agreement with the expected solution. Since IRBC is a simplified version of RBC, it offers a more computationally efficient implementation, making it a favorable choice for future simulations.

Based on these findings, the subsequent simulations were performed using second-order regularization combined with the IRBC boundary condition. Flows at Reynolds numbers $Re = 50{,}000$ and $Re = 100{,}000$ were

simulated under this setup. At such high Reynolds numbers, the flow becomes significantly more unstable compared to the validation cases, as illustrated in Fig. 1.

To analyze these flows, it is necessary to consider the concept of a statistically stationary regime, in which the overall behavior of the flow remains statistically constant over time. Once this condition is identified, a time average of the velocity field can be performed to extract the centerline velocity profiles.



(a) $Re = 50{,}000$ (b) $Re = 100{,}000$

Figure 6. The blue plot represents the value of u_x along vertical centerline, while the red plot represents the value of u_y towards the horizontal centerline

The results shown in Fig. 6 exhibit consistent and physically reasonable behavior. In particular, the velocity peak near the bottom wall decreases as the Reynolds number increases. This is attributed to the increasing chaotic motion within the cavity at higher Reynolds numbers, which shifts the dominant flow structures toward the center. This phenomenon is also discussed by Hegele Jr et al. [3] in the context of three-dimensional cavity flows at high Reynolds numbers.

It is important to note that true turbulence cannot be accurately represented in two-dimensional simulations due to the absence of vortex stretching, a fundamental mechanism in turbulent flows, which is inherently linked to the third spatial dimension.

Another noteworthy observation involves the performance analysis based on the mega lattice updates per second (MLUPS) metric. In the two-dimensional implementation on a GeForce RTX 4090, with single-precision floating-point arithmetic, MLUPS values vary significantly with grid resolution. Coarser grids, such as 128×128, exhibit relatively poor performance (400 MLUPS), while performance increases dramatically with refinement, reaching over 20,000 MLUPS for grids of size 1024×1024. Finer grids consistently achieve around 13,000 MLUPS across multiple simulations, indicating stable computational performance at higher resolutions.

5 Conclusions

This study presented a numerical investigation of two-dimensional lid-driven cavity (LDC) flows using the lattice Boltzmann method (LBM), with particular emphasis on high-order regularization and boundary condition treatments. The implementation was designed to balance accuracy and computational efficiency through CUDA-based GPU acceleration, moment-based collision modeling, and regularized formulations.

Validation against the benchmark results of Ghia et al. [19] confirmed the accuracy of the proposed approach for Reynolds numbers up to $10{,}000$, with excellent agreement in both steady-state behavior and velocity profiles. Grid refinement studies further demonstrated the convergence of the method, supported by kinetic energy plateau analysis and L_2 error metrics.

The application of high-order regularization revealed increased numerical complexity and energy fluctuations, requiring time-averaged velocity fields for consistent interpretation. Nevertheless, the technique showed promising accuracy near the boundaries and offers potential for extension to three-dimensional turbulence modeling.

Comparison between RBC and IRBC boundary conditions indicated that IRBC provides similar results while being computationally more efficient, making it the preferred option for future studies.

Finally, the performance analysis showed that finer grids lead to higher and more stable MLUPS values, indicating that the implementation scales well with resolution. The combination of second-order regularization and IRBC treatment proved suitable for simulating higher Reynolds numbers ($Re = 50{,}000$ and $100{,}000$), with velocity profiles obtained under statistically stationary conditions.

6 ACKNOWLEDGEMENTS

This study is part of the project "Experiment-based physical and numerical modeling of subsea oil jet dispersion", a cooperation agreement between UDESC and PETROBRAS (number 0050.0125248.23.9), governed by the investment clauses in P, D&I of the Brazilian National Agency of Petroleum, Natural Gas and Biofuels (ANP) (Resolution ANP 918/2023).

References

[1] L. D. Landau and others. Fluid mechanics: Landau and lifshitz. *Course of theoretical physics*, vol. 6, pp. 15–20, 2013.

[2] P. J. Pritchard and J. W. Mitchell. *Fox and McDonald's introduction to fluid mechanics*. John Wiley & Sons, 2016.

[3] L. Hegele Jr, A. Scagliarini, M. Sbragaglia, K. Mattila, P. Philippi, D. Puleri, J. Gounley, and A. Randles. High-reynolds-number turbulent cavity flow using the lattice boltzmann method. *Physical Review E*, vol. 98, n. 4, pp. 043302, 2018.

[4] M. A. Ferrari, de W. B. Oliveira Jr, A. Lugarini, A. T. Franco, and L. A. Hegele Jr. A graphic processing unit implementation for the moment representation of the lattice boltzmann method. *International Journal for Numerical Methods in Fluids*, vol. 95, n. 7, pp. 1076–1089, 2023.

[5] C. Coreixas, B. Chopard, and J. Latt. Comprehensive comparison of collision models in the lattice boltzmann framework: Theoretical investigations. *Physical Review E*, vol. 100, n. 3, pp. 033305, 2019.

[6] A. Montessori, G. Falcucci, P. Prestininzi, M. La Rocca, and S. Succi. Regularized lattice bhatnagar-gross-krook model for two-and three-dimensional cavity flow simulations. *Physical Review E*, vol. 89, n. 5, pp. 053317, 2014.

[7] J. Latt and B. Chopard. Lattice boltzmann method with regularized pre-collision distribution functions. *Mathematics and Computers in Simulation*, vol. 72, n. 2-6, pp. 165–168, 2006.

[8] M. Vardhan, J. Gounley, L. Hegele, E. W. Draeger, and A. Randles. Moment representation in the lattice boltzmann method on massively parallel hardware. In *Proceedings of the International Conference for High Performance Computing, Networking, Storage and Analysis*, pp. 1–21, 2019.

[9] M. Ferrari, A. Franco, and L. Hegele. Turbulent flow inside a cubic lid-driven cavity using moment representation lattice boltzmann method. *Physics of Fluids*, vol. 36, n. 7, 2024.

[10] C. Coreixas, G. Wissocq, G. Puigt, J.-F. Boussuge, and P. Sagaut. Recursive regularization step for high-order lattice boltzmann methods. *Physical Review E*, vol. 96, n. 3, pp. 033306, 2017.

[11] O. Malaspinas. Increasing stability and accuracy of the lattice boltzmann scheme: recursivity and regularization. *arXiv preprint arXiv:1505.06900*, 2015.

[12] K. K. Mattila, P. C. Philippi, and L. A. Hegele. High-order regularization in lattice-boltzmann equations. *Physics of Fluids*, vol. 29, n. 4, 2017.

[13] C. K. Aidun and J. R. Clausen. Lattice-boltzmann method for complex flows. *Annual review of fluid mechanics*, vol. 42, n. 1, pp. 439–472, 2010.

[14] X. Shan, X.-F. Yuan, and H. Chen. Kinetic theory representation of hydrodynamics: a way beyond the navier–stokes equation. *Journal of Fluid Mechanics*, vol. 550, pp. 413–441, 2006.

[15] S. Chen and G. D. Doolen. Lattice boltzmann method for fluid flows. *Annual review of fluid mechanics*, vol. 30, n. 1, pp. 329–364, 1998.

[16] J. Li. Chapman-enskog expansion in the lattice boltzmann method. *arXiv preprint arXiv:1512.02599*, 2015.

[17] T. Krüger, H. Kusumaatmaja, A. Kuzmin, O. Shardt, G. Silva, and E. M. Viggen. The lattice boltzmann method. *Springer International Publishing*, vol. 10, n. 978-3, pp. 4–15, 2017.

[18] J. Gounley, M. Vardhan, E. W. Draeger, P. Valero-Lara, S. V. Moore, and A. Randles. Propagation pattern for moment representation of the lattice boltzmann method. *IEEE Transactions on Parallel and Distributed Systems*, vol. 33, n. 3, pp. 642–653, 2021.

[19] U. Ghia, K. N. Ghia, and C. Shin. High-re solutions for incompressible flow using the navier-stokes equations and a multigrid method. *Journal of computational physics*, vol. 48, n. 3, pp. 387–411, 1982.